Pathways of Protoplanetary Disk Evolution and Dissipation

Elise Furlan
Spitzer Fellow,
Jet Propulsion Laboratory,
California Institute of Technology

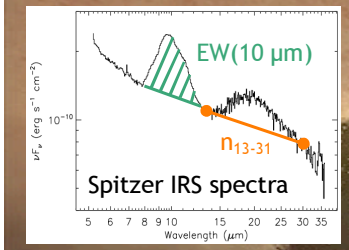

dust settling: depletion of small dust grains in upper disk layers by factors of 100-1000

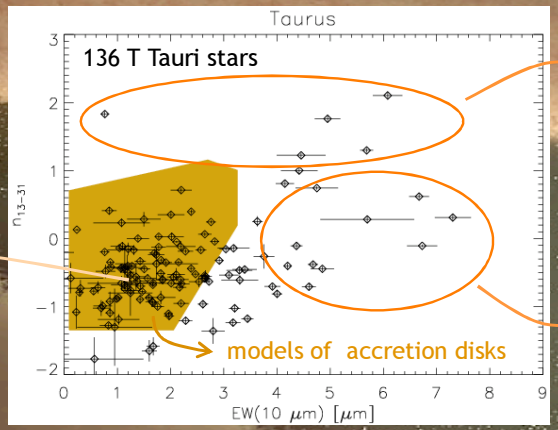

Furlan et al. (2006, 2009a)

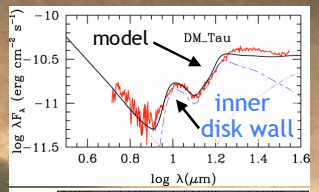

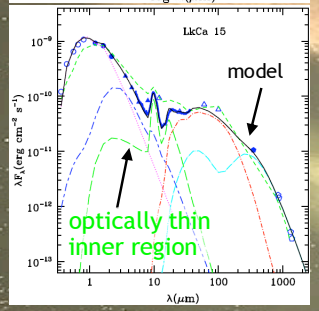

transitional disks: inner disk hole

Calvet et al. (2005)

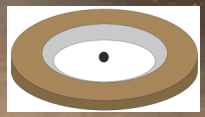

"pre"-transitional disks: disk gap within the optically thick disk

Espaillat et al. (2007b)

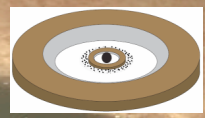

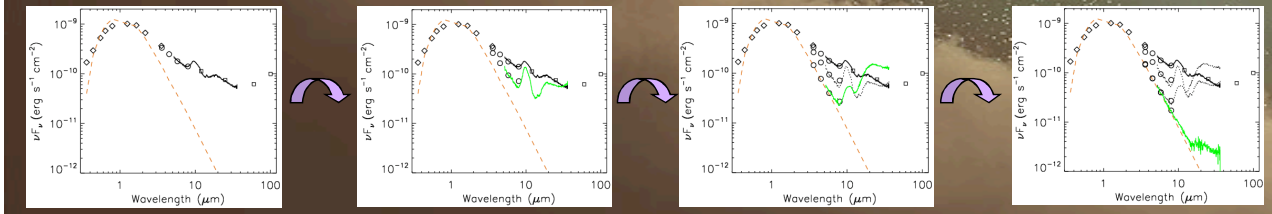

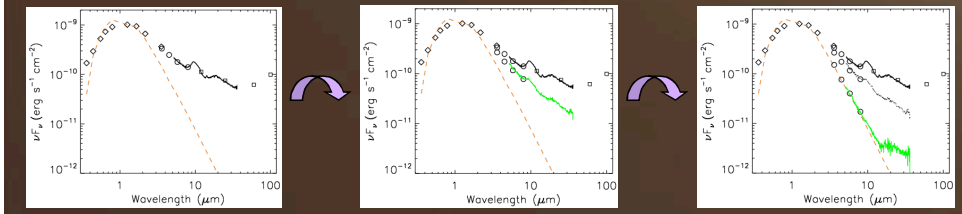

2 Pathways of Disk Dissipation?

- ➢ formation of inner gaps, holes, then dissipation of the disk from the inside out?
  - gaps: indicative of planet formation
  - inner (dust) holes: caused by dust growth, planets, photoevaporation, MRI-induced disk draining

→ different mechanisms likely operating in different disks and/or at different times

- ➢ steady depletion of material in the disk?

→ disk develops from flared to flat, optically thick, then to optically thin

→ main mechanism for late-type stars (with lower-mass disks)?

Spectroscopic analysis of CoRoT/Exoplanet fields

J.-C. Gazzano[1,2], M. Deleuil[1], P. De Laverny[2], C. Moutou[1], F. Bouchy[3,4], A. Recio-Blanco[2] ,A. Bijaoui[2]

Affiliations: (1) Laboratoire d'Astrophysique de Marseille (UMR 6110), OAMP, Université Aix-Marseille & CNRS, 38 rue Frédéric Joliot Curie, 13388 Marseille cedex 13, France, (2) Université de Nice - Sophia Antipolis, CNRS (UMR 6202), Cassiopée, Observatoire de la Côte d'Azur, BP 4229, 06304 Nice cedex 4, France, (3) Institut d'Astrophysique de Paris (UMR7095) CNRS, Université Pierre & Marie Curie, 98bis Bd Arago, 75014 Paris, France, (4) Observatoire de Haute-Provence, CNRS/OAMP, 04870 St Michel l'Observatoire, France

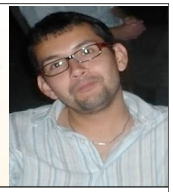

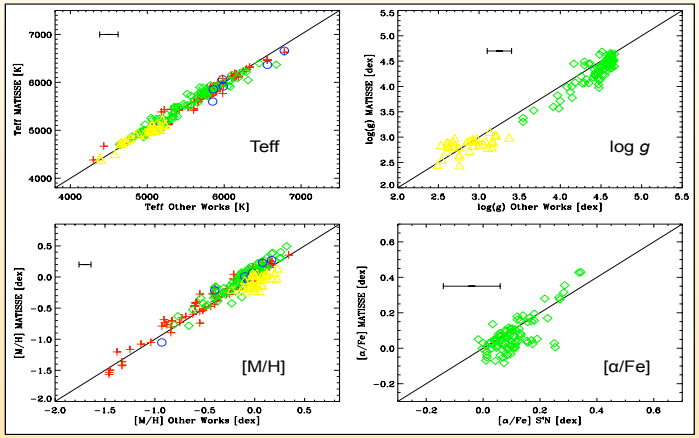

AUTOMATIC & HOMOGENEOUS Spectral Analysis for ~**1900** ***FLAMES/GIRAFFE*** spectra

V_{rad}, Teff, log g, [M/H], and [α/Fe] for 1227 stars in LRc01, SRc01 and LRa01

Basis for any study of **metallicity planet relation in CoRoT fields (Gazzano et al. 2010 Accepted)**

Properties of the planetary systems found by CoRoT.

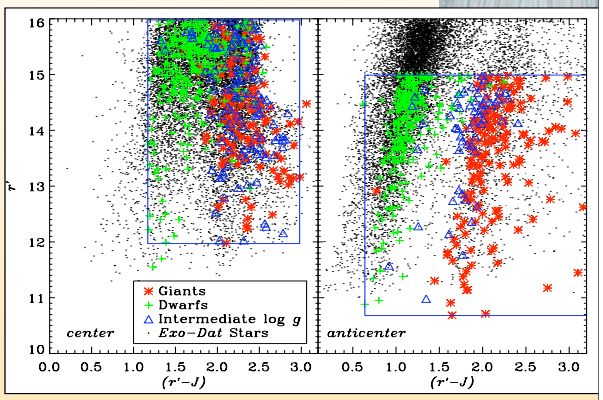

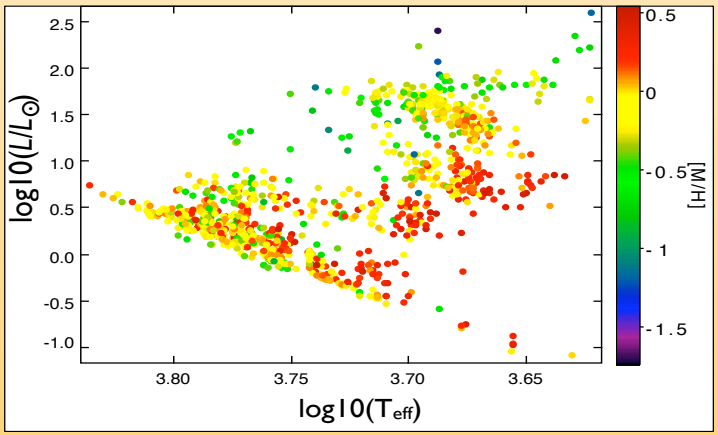

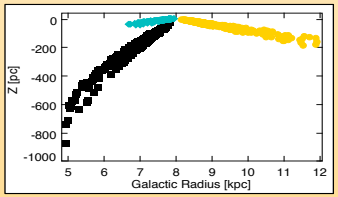

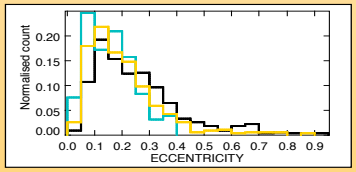

Galactic physics:

- **metallicity gradient** illustrated by the giants.
- **kinematics studies**

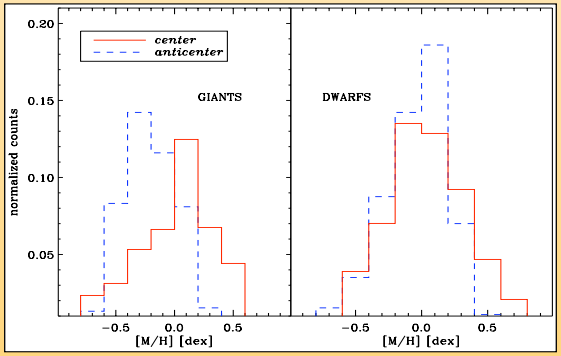

For information : jean-christophe.gazzano@oamp.fr

A PAthway towards the Characterization of Habitable Earths: the APACHE project

Paolo Giacobbe (University of Trieste/INAF)

APACHE is a project to undertake a long-term northern-hemisphere photometric survey to search for **transiting low-mass planets** orbiting a well-defined sample of **M dwarf stars** in the solar neighborhood. The main goals are:

The discovery and characterization of rocky planets in the *habitable zone* or, alternatively, constraining their occurrence rate;

The possibility to undertake in-depth characterization of the microvariabilty properties of a statistically significant sample of M dwarf stars

APACHE will monitor photometrically ~3500 nearby (d<40 pc) M dwarfs using an array of robotic telescopes at the **Astronomical Observatory of the Autonomous Region of the Aosta Valley** (OAVdA)

REFINING PHOTOMETRIC FOLLOWUP CAMPAIGNS BASED ON ORBITAL CONFIGURATIONS

Matthew J. Giguere, Debra A. Fischer
matthew.giguere@yale.edu

Introduction

While great developments have been made over the past 15 years in the understanding of planet formation and evolution, one area that remains to be fully unraveled is the role of eccentricity. Until the first exoplanets were detected, it was widely believed that all planets would be in near-circular orbits due to planet-disk interactions. That view was shattered, of course, by the first few observations of extrasolar planets. Today, the cause of planets in highly eccentric orbits is still not well understood. Planet-planet scattering simulations suggest that if high eccentricities are caused by interactions with other bodies in the system, then the angle between the spin axis of the host star and the orbital axis of the planet might be substantial. One way to observationally test this is to observe the host star spectroscopically while the planet transits (i.e., observe the Rossiter-McLaughlin Effect).

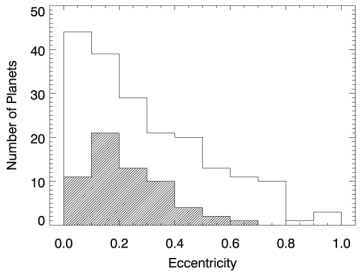

Figure 1. The distribution of planets detected via the transit and radial velocity methods to date. The shaded area represents candidates in multiple planet systems while the unshaded area represents systems where only one candidate has been detected.

Method

It is serendipitous that the same systems we are looking to observe transiting might also have a higher probability of transit. As seen in Figure 1, HD 17156b has a much higher probability of transit than if it were in a circular orbit with the same orbital period. Figure 3 shows the probability of transit as a function of orbital period for all the known candidates. From Figure 3 it is clear that the probability of transit is often higher when taking the eccentricity and omega into account. Taking all 5 known Keplerian parameters into account, we calculate the probability of transit and time of center transit and the photometric followup efforts are weighted with these considerations as described in Giguere et al. (2010).

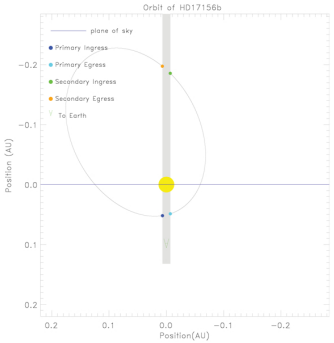

Figure 2. The inclination-projected orbit of HD 17156b as seen from the plane of the sky and perpendicular to the line of nodes. The Earth is towards the bottom-center of the plot. Because of the high eccentricity of this orbit and the favorable argument of periastron passage, the probability of transit of HD 17156b is much higher than it would have been if the planet were in a circular orbit with the same orbital configuration as given by Charbonneau (2007) in Equation 1.

$$P = 4.5 * 10^{-3} \left(\frac{1\mathrm{AU}}{a}\right) \left(\frac{R_* + R_{pl}}{R_{sun}}\right) \left[\frac{1 + e\cos\left(\frac{\pi}{2} - \omega\right)}{1 - e^2}\right] \quad (1)$$

Conclusions

While no transiting planets have been detected based on these methods to date, taking these factors into account has nevertheless lead to a more efficient use of telescope time for the followup photometry. Although that in itself is of great benefit, being a work in progress, these methods have the potential to show themselves as significantly more important.

Literature Cited

Charbonneau, D., et al., 2007, P&P V, 701
Giguere, M., et al., 2010, in prep

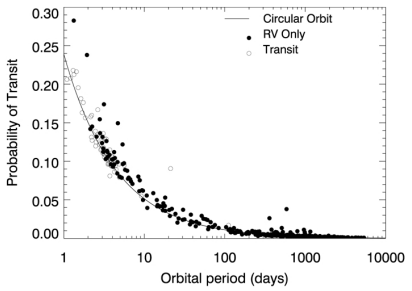

Figure 3. The probability of transit as a function of orbital period for the known distribution of exoplanets. The unfilled circles indicate that the candidate is known to transit while the filled circles are for candidates that have only been observed through Doppler observations. The solid line shows the probability for a circular orbit. It can be seen that taking all of the orbital parameters into account often leads to a higher probability.

White Dwarfs with an Infrared Excess

Jonathan Girven, Boris Gänsicke, Danny Steeghs, Carolyn Brinkworth and Detlev Koester

Over 400 planets are known around stars similar to that of our Sun, but what happens to these planets after the star ends its life and becomes a white dwarf?

1. Dusty Debris Disks and Brown Dwarf Companions

White dwarfs (WDs) are the most common stellar remnants in the Galaxy, having descended from main sequence stars with masses between 0.8 and 8 solar masses. The eventual fate of our Sun is to become a WD.

It has been found in rare cases that planets and small stellar companions can survive the red giant phase of the main sequence star and continue to orbit the compact stellar remnant (e.g. Farihi et al. 2009). Tidally disrupted asteroids are also believed to form disks around a small percentage of WDs (e.g. Gänsicke et al. 2006).

We aimed to perform a systematic search for WDs with an excess in the infrared, indicative of a second cool body, using large scale sky surveys. In the optical we used the Sloan Digital Sky Survey (SDSS) and in the infrared, the UKIRT Infrared Deep Sky Survey (UKIDSS). Follow up is then performed using the Spitzer Space Telescope.

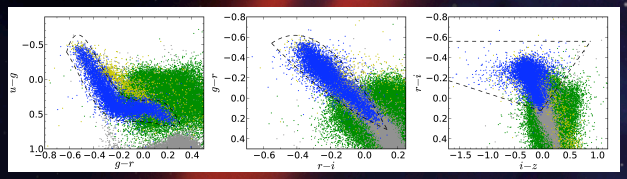

Optical SDSS *ugriz* colour-colour diagrams: DA WDs, other WDs, quasars and main sequence stars are marked as blue, yellow, green and grey respectively. The black dashed lines show the location in colour space of the designed selection criteria.

2. Selecting Hydrogen-Rich Atmosphere (DA) White Dwarfs

The SDSS database contains information on over 200 million stars. To select the relatively small population of DA WDs from this mass of objects, we use criteria on the optical colours. Colour-colour diagrams such as that above (effectively showing gradients in brightness as a function of wavelength) help design these criteria.

Gänsicke, B. T. et al., 2006, Science, 314, 1908
Farihi, J., Jura, M. Zuckerman, B., 2009, ApJ, 694, 805

Girven et al. (2010, in preparation)

3. Finding DA White Dwarfs with an Infrared Excess

Matching the optical data for the DA WDs with infrared data from UKIDSS results in photometry covering 3500 to 23000Å. Infrared colour-colour diagrams, such as that on the right, highlight stars which are brighter in the infrared than the majority of their single DA WD counterparts, indicating a second cool body.

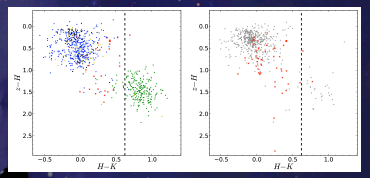

Above: Infrared z-H vs H-K colour-colour diagrams showing stars with SDSS spectroscopy for classification (left) and only photometry (right). DA WDs, other WDs, quasars, main sequence stars and photometric objects are marked as blue, yellow, green, black and grey respectively. Infrared excess objects are plotted as red crosses.

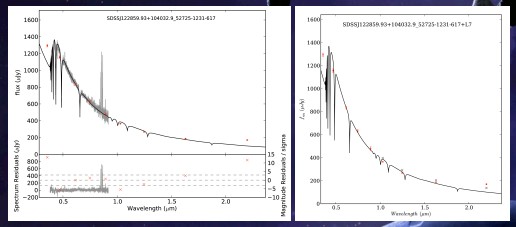

Left: Real (grey) and model (black) spectral energy distributions of SDSS J1228+1040: on the left showing the best fit model to the SDSS spectrum and on the right showing the same model with the addition of an L7-type companion as grey crosses. The real magnitudes are plotted in red.

4. Modelling the Excess

Fitting WD spectra allows us to obtain the effective temperatures and surface gravities. We can therefore extrapolate the spectral energy distribution (SED) into the infrared. Excesses over the predicted flux levels indicates a second object.

SDSS J1228+1040 (Gänsicke et al. 2006), in the SED displayed above, shows a clear (12 sigma) excess in the *K*-band (2.2μm) magnitude.

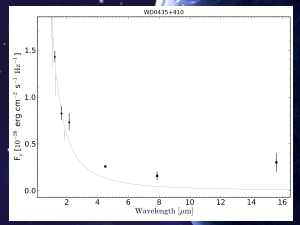

The infrared SED of the DAZ WD, WD0435+410. Black error bars show the 2MASS magnitudes at the shorter wavelengths as well as the Spitzer IRAC (4.5 and 8.0μm) and IRS (16μm) magnitudes. The grey line shows a model WD spectrum. The IR excess can clearly be seen at long wavelengths.

5. The Resulting Debris Disk Candidates

We have discovered that between 2 and 5% of DA WDs in our survey are estimated to have a late type companion or dusty debris disk. This is a lower limit for the total number because many disks will not be sufficiently bright to be detectable until the mid to far-infrared. Follow up observations with Spitzer can confirm the nature of the second bodies.

6. Spitzer Follow Up Observations

Observations with the Spitzer Space Telescope have been taken for a series of DA WDs with metal polluted atmospheres (DAZ WD). In the mid to far-infrared the contrast ratio between the WD and the disk becomes far more favourable towards seeing the disk. An example of this is show for WD0435+410 in the figure on the left. A clear excess can be seen in the far-infrared.

White dwarf stars offer an excellent environment for us to search for planets and their remnants.

Artist impression by Mark Garlick

Direct Imaging of Sub-Stellar Companions and Characterisation of the Brown Dwarf Desert

Janis Hagelberg, Geneva Observatory

Scientific goals

- Characterisation of the brown dwarf desert
- Atmospheric characterisation of brown dwarfs
- Preparation work for the SPHERE GTO

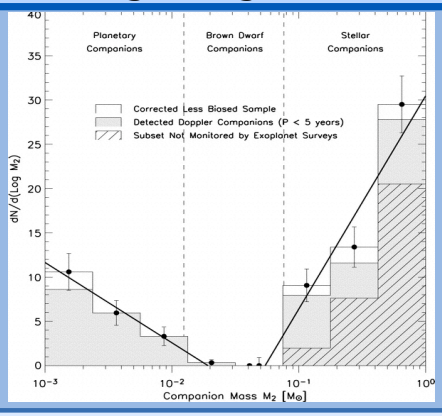

Mass distribution for companions of a sample of Sun-like stars within 50pc.
D. Grether and C.H. Lineweaver, ApJ 2006

Target selection

- Radial velocity drifts compatible with substellar companions and VLT/NACO adaptive optics detection limits are selected from the HARPS and CORALIE surveys.
- Monte-Carlo probability maps are generated for each candidate to determine detection probability in the mass-period diagram.

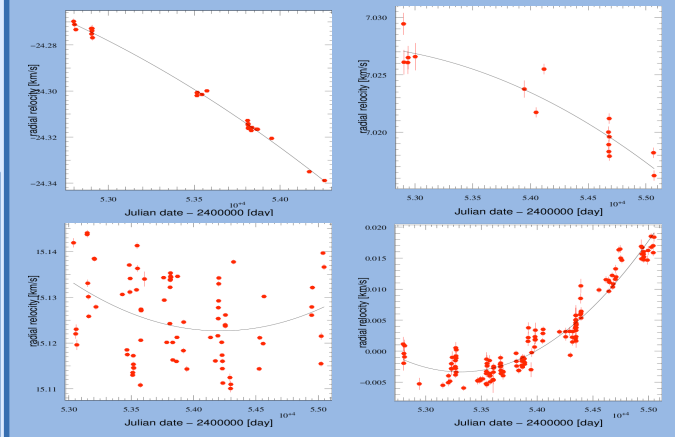

Figure 1:
RV drifts in HARPS with data points spread over up to seven years and precision below 1 m/s.

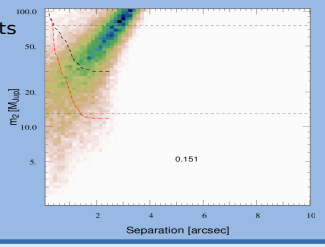

Figure 2:
Monte-Carlo probability map, with NACO L' band detection limits for 1Gyr (red) and 5Gyr (black) systems.

Detection method

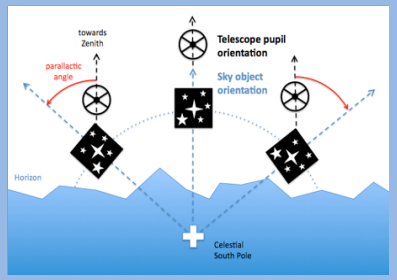

Courtesy of C. Thalmann

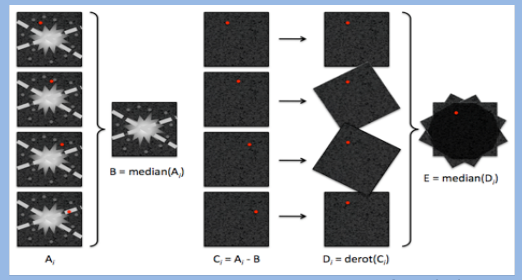

Courtesy of C. Thalmann

- In pupil tracking mode, the field rotates while observing the star.
- On the other hand, the telescope pupil, and artefacts linked to it stay fixed.

1) A median of the datacube is created
2) Only static parts remain in the median B
3) The median B is substracted from every single frame
4) The frames are derotated to correct for field rotation
5) The median of the derotated frames yields the final image.

Initial Results From Project 1640

Sasha Hinkley[1] (Caltech), Neil Zimmerman (Columbia University), Justin Crepp (Caltech), Ben R. Oppenheimer (AMNH), Lynne Hillenbrand (Caltech), Douglas Brenner (AMNH), Remi Soummer (STScI), Anand Sivaramakrishnan (STScI), Charles Beichman (NExScI/JPL, Ian R. Parry (IoA Cambridge), David L. King (IoA Cambridge), Lewis C. Roberts Jr. (JPL), Antonin Bouchez (Caltech), Jennifer Roberts (Caltech), Richard Dekany (Caltech), Rick Burruss (JPL), Michael Shao (JPL), Gautam Vasisht (JPL).

Abstract: Project 1640 represents a long-term high contrast imaging effort at the 200-inch Hale telescope at Palomar observatory. We aim to obtain imaging and spectroscopy of brown dwarf and exoplanetary mass companions to nearby stars. The Project utilizes a diffraction-limited apodized pupil Lyot coronagraph that has been integrated with a lenslet based integral field spectrograph. This entire package is mounted on the 241-actuator Shack Hartmann based Adaptive Optics system on the Hale Telescope (see right). The spectrograph operates in the J and H passbands (1.05 - 1.75 μm) and we achieve somewhat low spectral resolution ($\lambda/\Delta\lambda$ ~ 23). However, the wavelength diversity provided by our spectral resolution allows for speckle suppression using the LOCI algorithm to increase our sensitivity by 2 to 3 magnitudes (see lower right). For the initial phase of the project, we are undertaking a survey of nearby stars, focusing primarily on a complete survey of A-stars with the existing AO system. In 2010, after the implementation of an internal wave front calibration system and an upgrade to a 3000-actuator AO system at Palomar, we will undertake a much longer 99-night survey on the 200-inch.

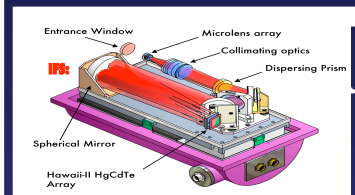

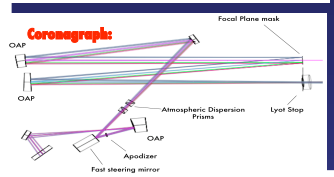

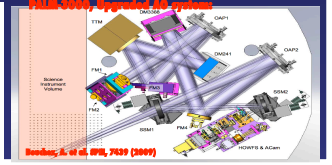

An M Dwarf Orbiting ζ Virginis

Hinkley et al (2010a)

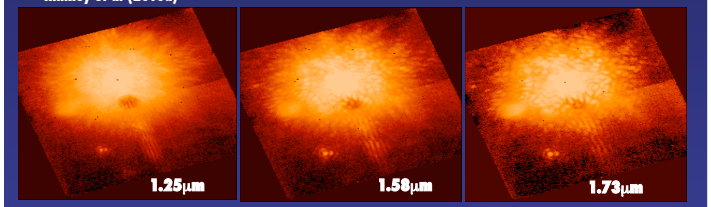

Common Proper motion confirmed by nearly 5 years of coverage, showing orbital motion

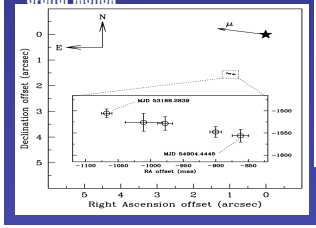

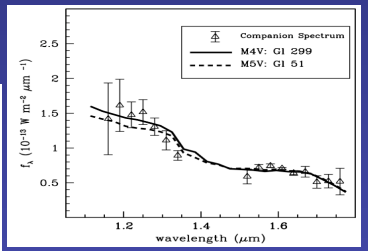

J and H band spectra are consistent with a mid-M dwarf star, of roughly 0.16 solar masses. This gives a very low mass ratio of ~0.08

Speckle Suppression through Wavelength Diversity

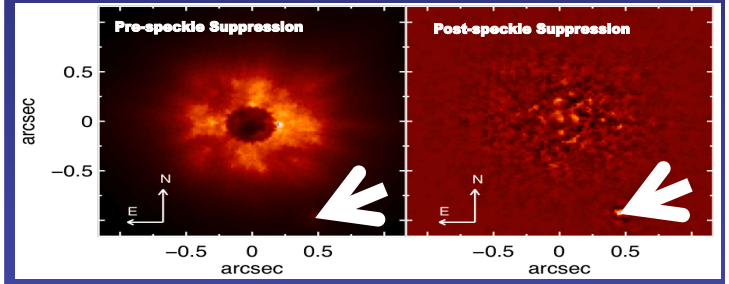

See Crepp et al. (2010, forthcoming) & Pueyo et al (2010, forthcoming)

[1]Sagan Fellow. A portion of this work was performed under a contract with the California Institute of Technology (Caltech) funded by NASA through the Sagan Fellowship Program. A portion of this work was carried out at the Jet Propulsion Laboratory, California Institute of Technology, under a contract with NASA.

The Rossiter-McLaughlin Effect for Transiting Extrasolar Planetary Systems: New Theory and Observation

Teruyuki Hirano (The Univ. of Tokyo)

Introduction

- Transiting exoplanetary systems are particularly interesting targets since we can learn many physical parameters of the systems, which are otherwise unavailable.
- "The Rossiter-McLaughlin effect" (the RM effect) is one of such gifts from transiting exoplanetary systems.
- During a planetary transit, stellar absorption lines are distorted due to a partial occultation of the rotating stellar disk by the planet. (The red solid line in Figure 1 indicates the line profile during a transit).
- When we observe radial velocities (RVs) of a transiting system, we detect an apparent RV anomaly due to the line distortion. (See Figure 2.)
- The RV anomaly against time depends on the trajectory of the transiting planet. We show the two cases of RV anomaly curves in Figure 2.
- Thus, by carefully measuring the RV anomaly during a transit, one can estimate the sky projected angle between the stellar spin axis and the planetary orbital axis (denoted by λ). (See Figure 3.)
- This angle λ is important when we discuss planetary formation/ migration theories. Many samples of λ are necessary in order to compare observational results with theoretical predictions.
- Observational results to date are shown in Figure 4 (histogram of λ). While in more than half of the systems the stellar spin axis and planetary orbital axis are well aligned, some systems show significant spin-orbit misalignments.
- In this poster, I present new analytical description of the RM effect, and also give the newest observational results.

Fig.1

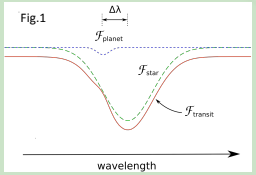

Fig.2

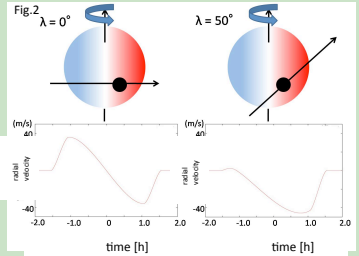

Fig.3

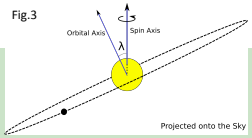

Fig.4

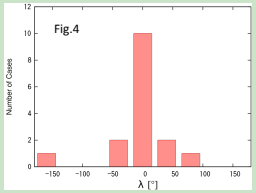

Analytic Description of the RM Effect

- In order to estimate the spin-orbit misalignment angle λ, a relation between observed radial velocity anomalies and position of the planet is required.
- Previously, Ohta et al. 2005 derived an analytic formula for the RM effect. However, it was shown that the formula deviates from the simulated results (Winn et al. 2005).
- We point out a problem in the derivation of the analytic formula by Ohta et al., and re-derived an analytic expression for the RV anomaly during a transit. (Hirano et al. 2010)

Previous Formulation (based on the moment method)

The center of the line of the distorted line during transit is estimated from the first moment (the center of gravity):

Calculating $\delta_{\rm RM} \equiv \frac{\int_{-\infty}^{\infty} \lambda \mathcal{F}_{\rm transit}(\lambda) d\lambda}{\int_{-\infty}^{\infty} \mathcal{F}_{\rm transit}(\lambda) d\lambda}$ we obtain $\delta_{\rm RM} = -\frac{f}{1-f}\Delta\lambda$

where $\delta_{\rm RM}$ indicates the wavelength anomaly of the center of the absorption line, and can be translated into the RV "anomaly".

However, this result based on the moment method could not explain "observed" RV anomalies.

New Formulation (based on the cross-correlation method)

We cross-correlated the distorted spectrum with a stellar template spectrum and estimated the best-fit position. This "cross-correlation" method is used in actual RV data analysis.

Calculating $\left.\frac{dC(x)}{dx}\right|_{x=\delta_{\rm RM}} = 0,$ $C(x) = \int_{-\infty}^{\infty} \mathcal{F}_{\rm star}(\lambda - x)\mathcal{F}_{\rm transit}(\lambda) d\lambda$ we obtain $\delta_{\rm RM} \approx -f \frac{\int_0^{\infty} \exp[-2\pi^2\beta^2\sigma^2 - 4\pi\gamma\sigma]\tilde{R}(\sigma)\sigma\sin(2\pi\sigma\Delta\lambda)d\sigma}{2\pi\int_0^{\infty} \exp[-2\pi^2\beta^2\sigma^2 - 4\pi\gamma\sigma]\left\{\tilde{R}(\sigma)\right\}^2\sigma^2 d\sigma}$

where $\tilde{R}(\sigma)$ is the Fourier transform of rotational broadening kernel for stellar absorption lines, and β and γ is the intrinsic line width parameters.

We showed that this new analytic formula is in better agreement with the simulated RV anomalies (Hirano et al. 2010)

New Observation of the RM Effect

- We have observed the RM effect for several systems using Subaru telescope. With Subaru/HDS, we can typically attain RV precision of ~3 m/s, which is sufficient for the detection of the RM effect in most of the transiting systems.
- Systems with large eccentricities are especially of great interest because it is reported that such systems are highly likely to have large spin-orbit misalignment angle λ.
- Thus, we conducted an observation of HAT-P-11b, whose eccentricity was reported to be ~0.2.

Target:
- Name: HAT-P-11
- Spectral Type: K4
- Planetary Radius: 0.0576 ± 0.0009 R_J
- Stellar Rotational Velocity: v sin i = 1.5 ± 1.5 km/s
- Orbital Eccentricity: 0.198 ± 0.046 (Bakos et al. 2010)

Observation:
- Date: May 20, May 26 (transit), June 30 in 2010
- Instrument: Subaru/HDS
- Spectral Resolution: R~45,000 (May) or 90,000 (June)

Results: We combined the RV data we took with the published data-set by Bakos et al. (2010). The (preliminary) RV results are shown in Figure (a). Figure (b) shows the RVs around the transit phase. The best-fit parameters to describe the observed RVs are as follows:
- RV semi-amplitude: K = 12.3 ± 1.1 m/s
- Spin-orbit misalignment angle: λ = 103° ± 28°
- Orbital Eccentricity: 0.22 ± 0.04

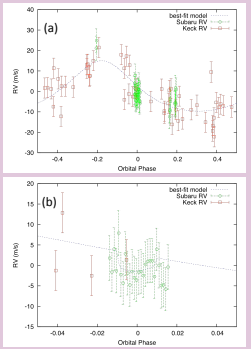

This is the first detection of the RM effect for a Neptune-size planet!

Hirano et al. 2010 in prep.

Middle Cambrian Surface Apatite Dissolution: A Mycorrhizal Fungi Biosignature?

Lev Horodyskyj

Formerly of Pennsylvania State University, working with Lee Kump and Tim White

Introduction

Soils form on sediments and bedrock exposed to the atmosphere, and can record the effects of various processes, including changes in moisture content, temperature, and biological activity, which acted upon soil prior to burial. Although paleosols (ancient soils) can be subject to post-burial alteration, careful analysis of paleosols can yield information about the conditions in which they developed.

Several Middle Cambrian (>504 Ma) paleosols from drill cores throughout the US Midcontinent Region were analyzed to understand Middle Cambrian weathering and to determine if a terrestrial biota was present at this time.

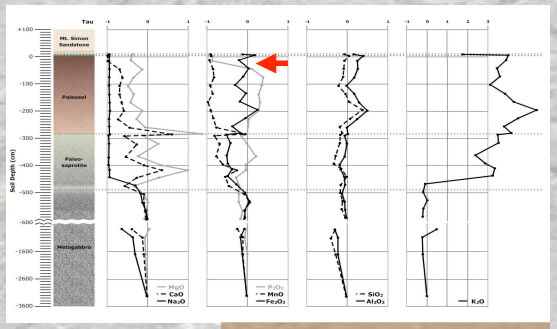

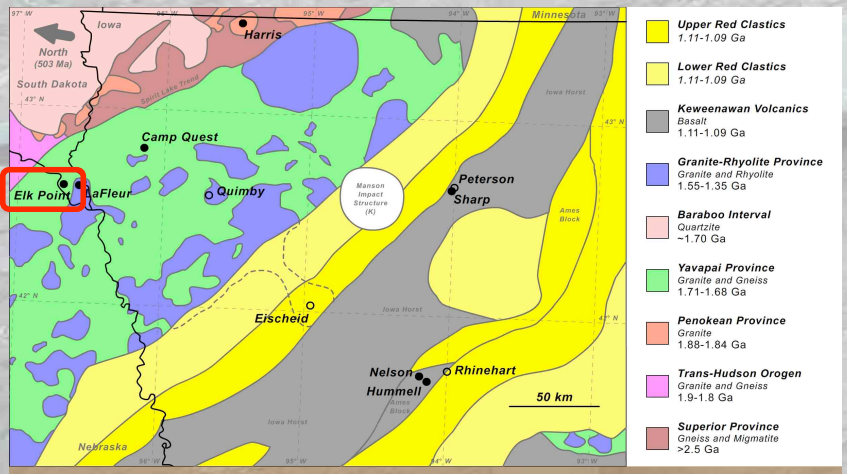

Study Area

The US Midcontinent region consists of a variety of Archean and Proterozoic terranes that were exposed to the atmosphere and subject to weathering. All locations are overlain by the >504 Mt. Simon Sandstone. The Elk Point paleosol yielded the most interesting results

Results

Oxide results are normalized to immobile Ti. Cation losses (Na, Ca, Mg) are typical of soil environments. Fe, Al, and Si immobility is likewise typical of weathering under an oxidizing atmosphere. K enrichment is likely a result of metasomatic fluid migration. Enrichment of Ca and Mg is a result of soil carbonates (which form at the average depth of wetting) later dolomitized by metasomatic fluids. The most significant pattern here is the **surface depletion of P**.

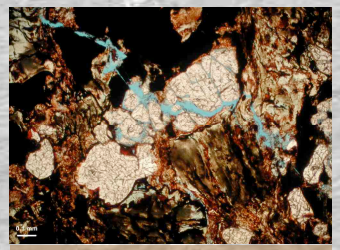

Heavily weathered apatite grain at -36 cm

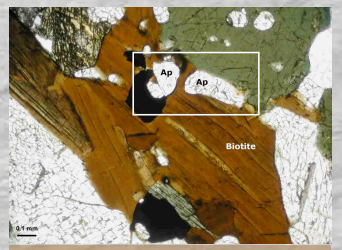

Unweathered apatite grain at -1576 cm

Apatite Dissolution

Apatite [$Ca_5(PO_4)_3(F,Cl,OH)$], is relatively stable in soils. Dissolution can be enhanced by acidic conditions or organic acids. Inorganic dissolution results in the precipitation of secondary phosphates. Secondary phosphate precipitation can be suppressed by biological P uptake. Note dissolution of apatite crystals without the formation of rinds or secondary precipitates.

Conclusions

The Elk Point paleosol shows elemental mobilizations that are typical of soils. However, P has been notably removed from the surface layers. P is a limiting nutrient in terrestrial environments, as it can only be accessed through dissolution of recalcitrant P-bearing minerals, such as apatite. Apatite at Elk Point is mostly unweathered, except near the surface. The lack of secondary phosphates or mobilization of P down-section indicates P uptake. The presence of argillans in the zone of apatite dissolution is likely a result of high soil Ca^{2+} concentrations, as carbonates at depth indicate water penetration >3 m into the soil. P uptake resulting in high Ca^{2+} soil concentrations has been previously associated with the activity of mycorrhizal fungi (plant-associated symbiotic fungi). The presence of mycorrhizal fungi in the Middle Cambrian may have contributed to enhanced weathering during this time.

Argillan Formation

Clays are formed by chemical weathering of rock minerals. Mobilized clays can be transported deeper into soils, where they can be immobilized in zones of desiccation or high cation concentrations. Clays at Elk Point are concentrated between 13-37 cm, a zone that coincides with the apatite dissolution zone. Dissolution of apatite would have resulted in high Ca^{2+} soil concentrations

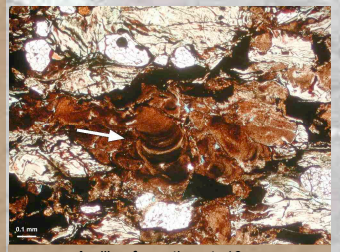

Argillan formation at -16 cm

SEARCH FOR EXOPLANETS USING TTVS IN THE SOUTHERN HEMISPHERE

Sergio Hoyer, Patricio Rojo

Universidad de Chile. Astronomy Department.

The method of **Transit Timing Variations (TTVs)** can detect additional low-mass planets in transiting exoplanetary systems. Those low-mass planets are in principle undetectable by other methods like RVs. In 2008 we started an homogeneous monitoring of known transiting planets in the Southern Hemisphere with observations of a cadence of 20 to 50 seconds. By carefully measuring the central time we are able to detect long- and short-term variations of the primary transits, and therefore infer the presence of additional bodies in those systems.

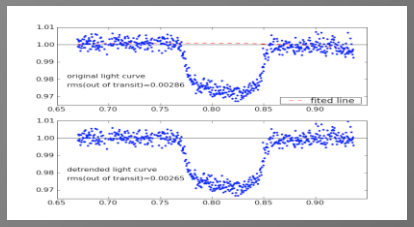

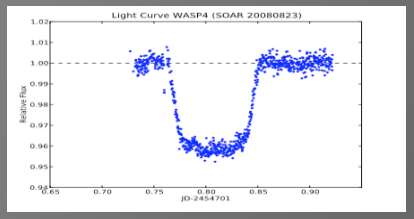

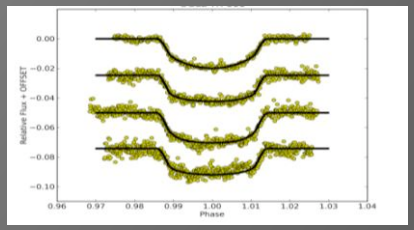

Preliminary light curves we are obtaining to measure the central time of the transits and other physical parameters.

shoyer@das.uchile.cl

http://www.das.uchile.cl/~shoyer

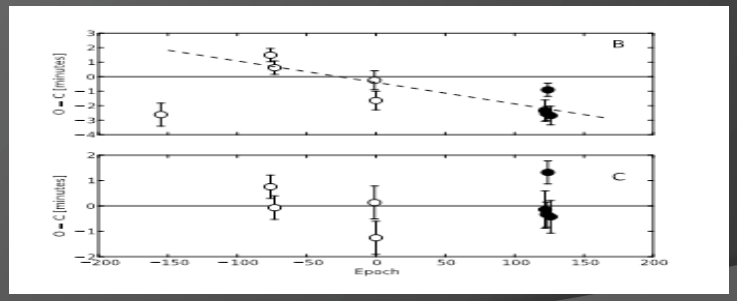

Preliminary *Observed minus Calculated* diagram of the central times of the transits for OGLE-TR-111b.

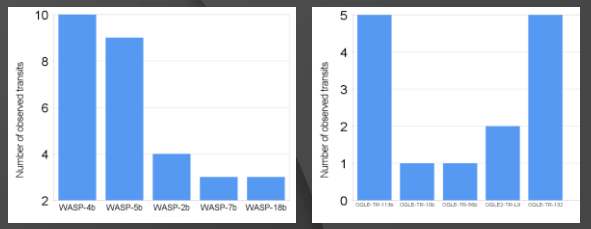

Number of observed transit by our project.

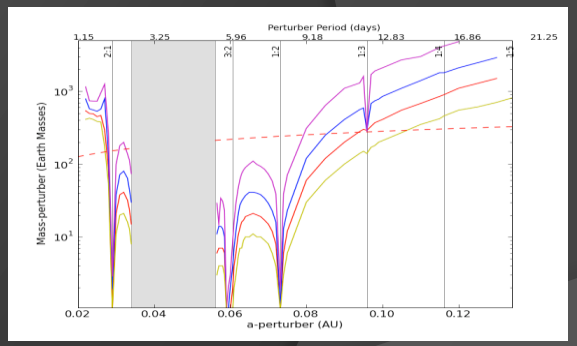

Example of mass limits for an unseen orbital perturber we can obtain using information from TTVs.

We acknowledge support from FONDAP (Project 1501003).